Please cite this article in press as: Funabiki et al., Autoimmune Disorders Associated with Gain of Function of the Intracellular Sensor MDA5, Immunity (2014), http://dx.doi.org/10.1016/j.immuni.2013.12.014

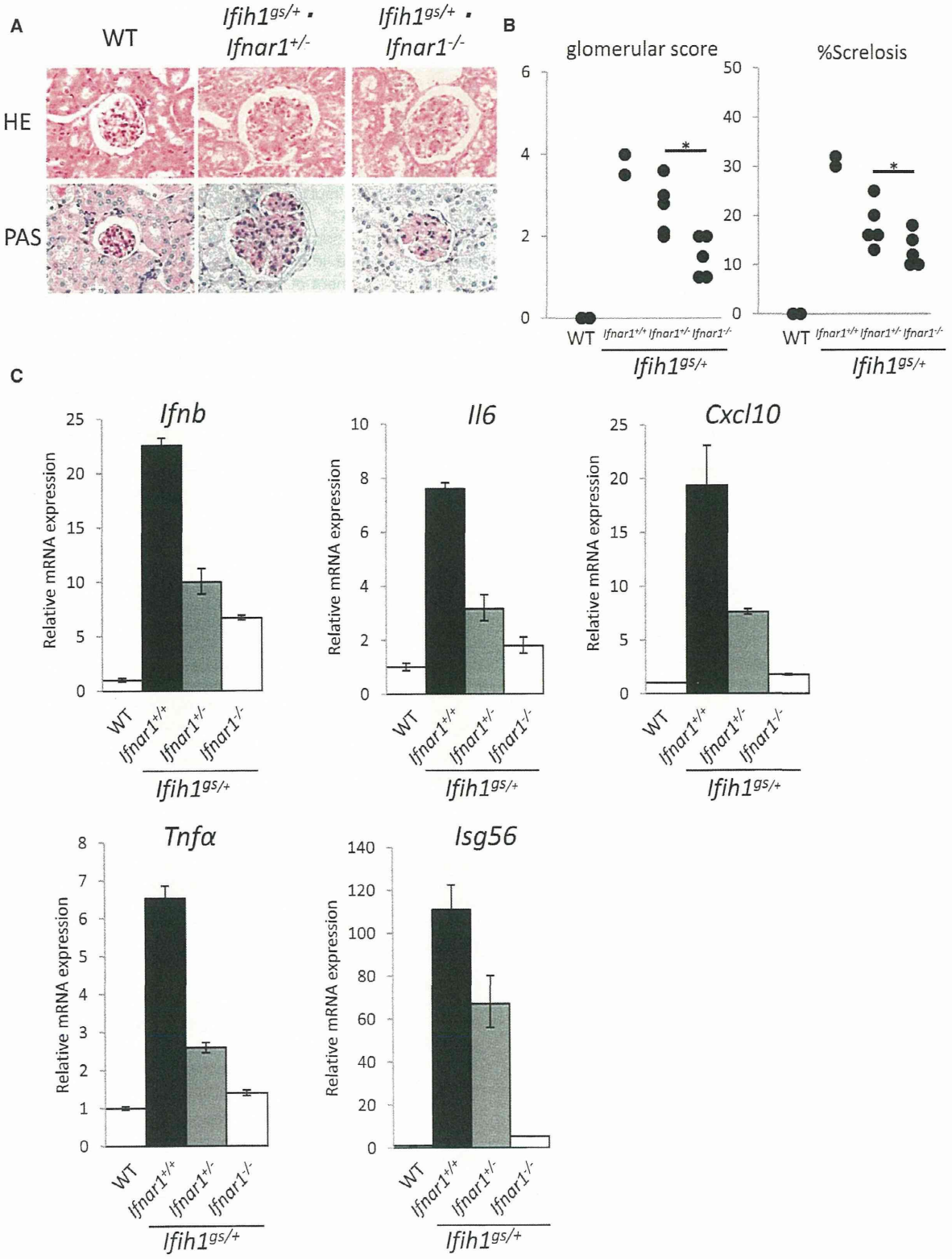

(legend on next page)

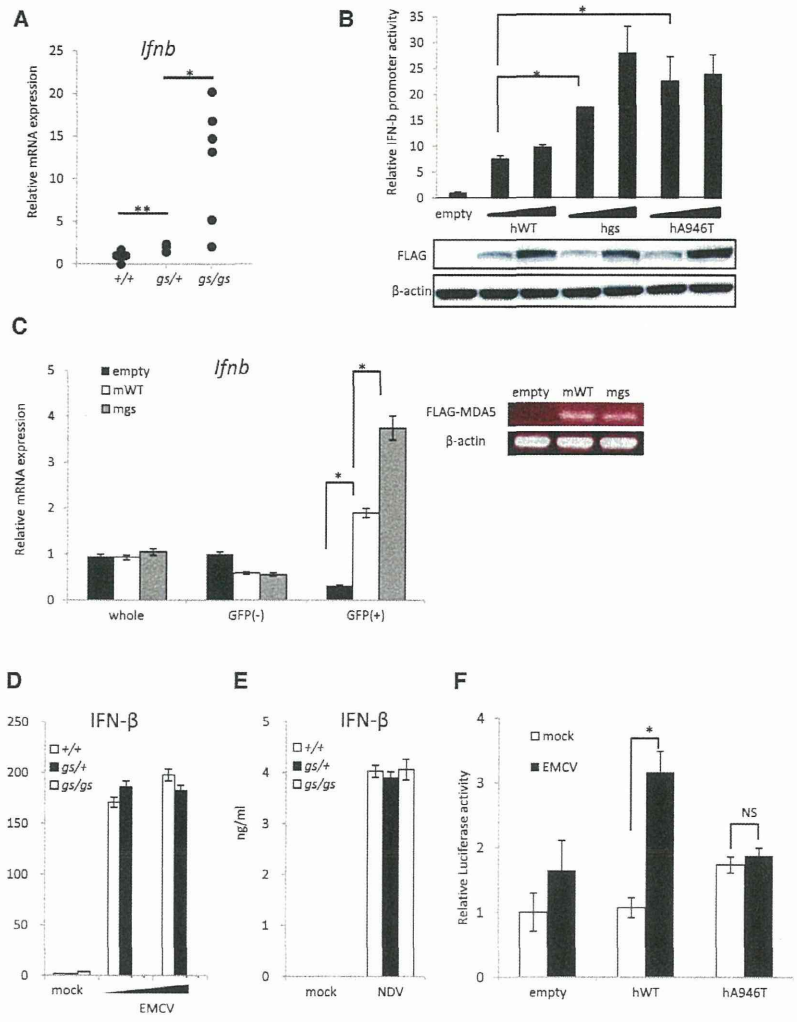

Figure 6. G821S Mutation of MDA5 Is Unresponsive to RNA Ligands but Constitutively Active

(A) Basal *Ifnb* mRNA level in MEFs are shown. Data are shown as mean ± SD of duplicate samples. Statistical significance was determined by Student's t test. *p < 0.03, **p < 0.05.

(B) Huh7 cells were transfected with a reporter gene (p-55C1B Luc) and empty vector (BOS) or expression vectors for FLAG-tagged human MDA5 and MDA5 mutants. Forty-eight hr after the transfection, luciferase activity was determined and indicated protein expression was accessed in SDS-PAGE. Statistical significance was determined by Student's t test. *p < 0.03.

(C) *Ifnb* mRNA levels in GM-CSF induced DCs expressing WT MDA5 and MDA5 gs. The DCs were infected with retroviruses, which introduce indicated genes and GFP independently. Forty-eight hr after infection, they were sorted according to GFP expression by FACS and subjected to quantitative real-time PCR. Data are shown as mean ± SD of duplicate samples of a representative from two independent experiments. Indicated gene expression in GFP (+) cells was shown by RT-PCR in the right panel. Statistical significance was determined by Student's t test. *p < 0.03.

(D and E) IFN-β concentration in culture supernatant from MEFs infected with various titer of EMCV (D) or NDV (E) for 24 hr were measured by ELISA. Data are shown as mean ± SD of duplicate samples of a representative from three independent experiments.

(F) *Ifih1*$^{-/-}$ MEFs were transfected with empty vector or expression vector for human WT MDA5 or MDA5 A946T and a reporter, p-55C1B Luc. Forty-eight hr after the transfection, the cells were infected with EMCV for 6 hr and IFN-β promoter activity was determined. Statistical significance was determined by Student's t test. *p < 0.05.

In summary, we describe the mechanisms of how MDA5 G821S mutation contributes to autoimmunity in a mouse model and how human SNP of MDA5 A946T potentially associates to autoimmune disorder. These findings provide insights into how dysregulation of cell-intrinsic antiviral sensors leads to autoimmunity and suggest approaches for therapeutic opportunities.

EXPERIMENTAL PROCEDURES

Mice

Ifih1$^{gs/+}$ mice with a DBA/2 background were proliferated by in vitro fertilization of *Ifih1*$^{gs/+}$ sperm × DBA/2JJcl female ovum. Heterozygotes of G821S MDA5 mutant with a DBA/2 background were analyzed as stated. Neither sex nor litter effects were detected by ANOVA in the survival rate and histological analysis and so data from different sexes and litters were analyzed together. *Mavs*$^{-/-}$ mice were kindly provided from S. Akira (Osaka University) and *Ifnar1*$^{-/-}$ mice were purchased from B&K Universal. All animal experiments were conducted in compliance with regulations approved by the Committee for Animal Experiments of the Institute for Virus Research, Kyoto University.

Cells, Virus, and Reagents

MEFs were prepared from 12.5–13.5 embryos generated by in vitro fertilization of *Ifih1*$^{gs/+}$ × *Ifih1*$^{gs/+}$ with a DBA/2JJcl background and cultured in Dulbecco's modified Eagle's medium (DMEM) with fetal bovine serum (FBS) and penicillin-streptomycin (100 U/ml and 100 μg/ml, respectively). To prepare GM-CSF-induced BMDCs, we prepared bone marrow cells from femora and tibia of 3- to 10-week-old mice. Cells were cultured in RPMI 1640 medium supplemented with 10% FBS, 100 μM 2-ME, and 10 ng/ml murine GM-CSF (Peprotech). Medium was changed every 2 days. Encephalomyocarditis virus (EMCV) was purchased from ATCC.

Figure 5. Type I IFNs Are Partially Responsible but not Essential for MDA-5 Dependent Nephritis

(A) Histology of kidney from WT, *Ifih1*$^{gs/+}$, *Ifnar1*$^{+/-}$, or *Ifnar1*$^{-/-}$ mice (left panels, Haematoxylin-eosin staining; right panels, PAS).

(B) Histological scores and percentage of sclerosis in kidney from WT, *Ifih1*$^{gs/+}$, *Ifnar1*$^{+/+}$, *Ifnar1*$^{+/-}$, or *Ifnar1*$^{-/-}$ mice were evaluated. Statistical significance was determined by Student's t test. *p < 0.03.

(C) Indicated mRNA gene-expression levels in kidney from *Ifih1*$^{gs/+}$, *Ifnar1*$^{+/+}$, *Ifnar1*$^{+/-}$, or *Ifnar1*$^{-/-}$ mice were determined by quantitative real-time PCR. Littermate mice were subjected and data are shown as mean ± SD of duplicate samples of a representative from three independent experiments.

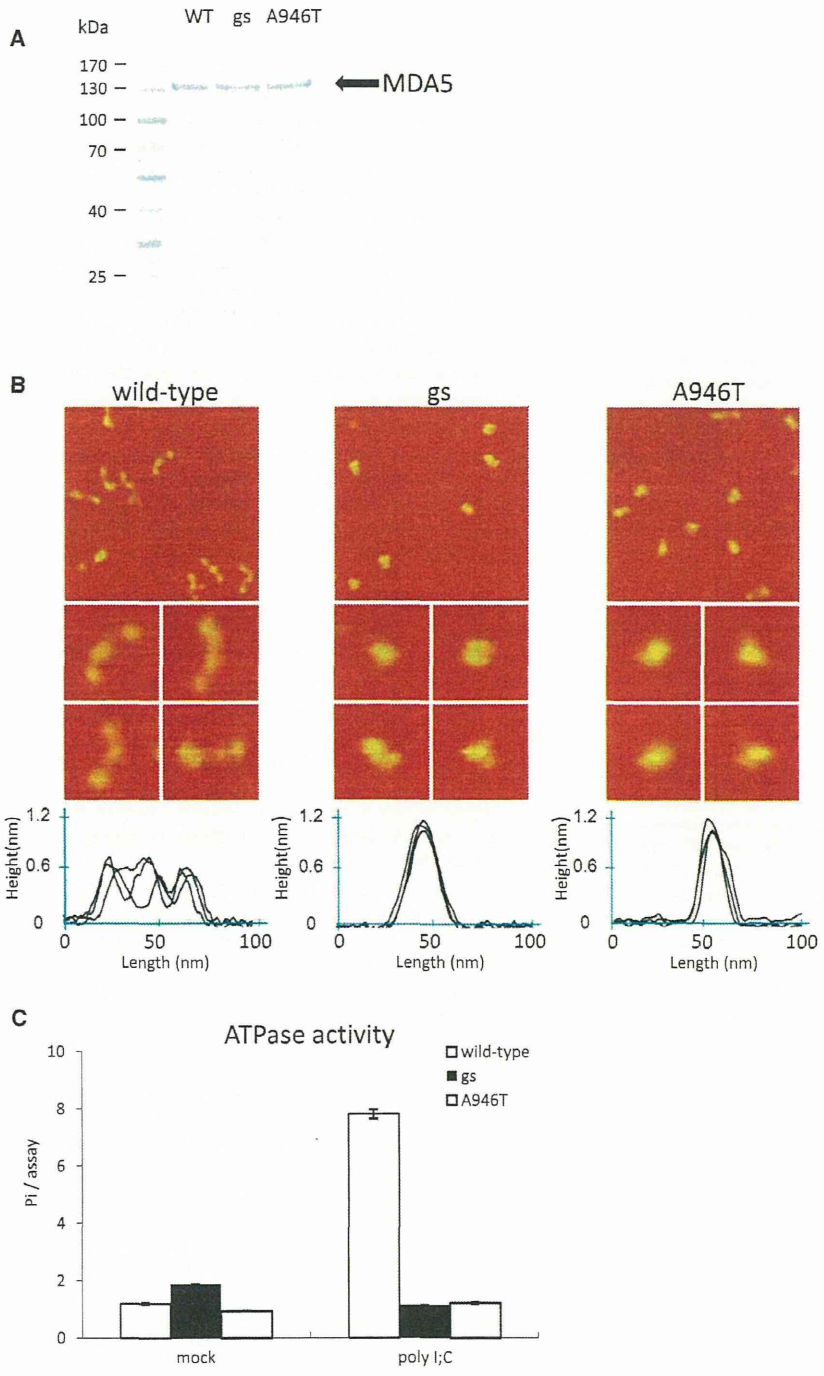

Figure 7. G821S and A946T Mutations Lead to Conformational Change and Abrogate ATPase Activity of MDA5

(A) Purity of MDA5 recombinant protein by SDS PAGE.

(B) Single-molecule analyses of the WT and mutant MDA5 molecules by AFM. Top images were obtained from 500 nm scans. Middle shows four individual molecules each in the WT and mutant images are marked by arrow heads and depicted in 100 nm zoomed-in scales. Bottom shows section analyses where four individual height features from the middle panels were superimposed, illustrating the height differences between the WT and mutant molecules.

(C) ATPase activity of WT and mutant MDA5. ATPase activity of the recombinant WT and mutant MDA5 proteins were determined in the absence or presence of polyI:C. Data are the mean ± SD of duplicate samples of a representative of three independent experiments.

PRISM 7700 sequence detection system (Applied Biosystems) or the STEP One plus Real Time PCR system (Applied Biosystems) and TaqMan Fast Universal PCR Master Mix (Applied Biosystems). TaqMan primers for mouse Ifnb1, IL-6, Cxcl10, Isg56, Tnfa, and 18 s rRNA were purchased from Applied Biosystems. The RNA copy numbers were normalized to that of internal 18 s rRNA.

Flow Cytometry

Cell suspensions of the spleen were prepared by sieving and gentle pipetting, and were treated with red cell lysis. For surface staining, cells were maintained in the dark at 4°C throughout. Cells were washed in ice-cold PBS, then incubated with each antibody for 15 min and washed twice with PBS. Antibodies for flow cytometry were purchased from BioLegend, eBioscience, and BD Biosciences. Data were acquired on the FACS Canto II flow cytometer (BD Biosciences) and analyzed with FlowJo.

Bone Marrow Chimeras

WT mice with a DBA/2JJcl background were irradiated with 8 Gy. Bone marrow cells from *Ifih1*$^{+/+}$ or *Ifih1*$^{gs/+}$ mice were infused intravenously 6 hr after irradiation. Mice were treated with antibiotics for 12 days after irradiation. To assess chimerism, we determined the abundance of WT and MDA5 mutant alleles in genomic DNA obtained from the spleen by PCR.

Plasmid Construct

The p-55 C1B Luc, pEF-BOS-FLAG MDA5 has been described previously (Shigemoto et al., 2009). pEF-BOS-FLAG-MDA5 G821S, A946T were constructed by introducing the mutations into pEF-BOS-FLAG MDA5 respectively with the KOD-Plus-Mutagenesis Kit (TOYOBO).

Histological Analysis

Tissues were fixed in 10% formalin, paraffin embedded, cut into sections (5 μm), and stained with hematoxylin-eosin or Periodic acid-Schiff.

Quantitative Real-Time PCR

Total RNA was prepared with TRIzol reagent (Invitrogen), treated with DNase I (Roche Diagnostics), and reverse-transcribed with a High-Capacity cDNA Reverse Transcription Kit (Applied Biosystems) according to the manufacturer's instructions. Reverse transcription-PCR was performed with the ABI

Retroviral Expression

pLZR-IRES/GFP vector has been described previously (Satoh et al., 2010). A murine WT MDA5 or MDA5 G821S cDNA was cloned into the pLZR-IRES/GFP retroviral vector. The constructs were transfected into the packaging cell line PlatE, and viral supernatants were collected 48 hr after transfection.

Measurement of IFN-β Production

Cells were infected with EMCV, NDV for the indicated period. Culture supernatants were collected and analyzed for IFN-β with an enzyme-linked immunosorbent assay (ELISA). ELISA kit for mouse IFN-β was purchased from PBL Biochemical Laboratories.

Luciferase Reporter Assay

The Dual-Luciferase Reporter Assay System (Promega) was used according to the manufacturer's instructions for luciferase assays. As an internal control, the Renilla Luciferase construct pRL-TK (Promega) was used.

Protein Purification

The cDNA encoding human WT MDA5, MDA5 G821S, or A946T was inserted into pAcGHLT-B vector (BD Biosciences). To obtain recombinant baculoviruses, Sf9 insect cells were cotransfected with the expression plasmid and BD Baculo Gold Linearized Baculovirus DNA (BD Biosciences) according to the manufacturer's protocol. The recombinant MDA5 proteins were expressed in Sf9 or High five insect cells (2×10^7 cells/150 mm dish) by infection with recombinant baculovirus for 4 days. The cells were lysed in lysis buffer (50 mM Tris–HCl pH 8.0, 150 mM NaCl, 1.5 mM DTT, 1% Triton X-100) with protease inhibitor cocktail (Nacalai Tesque). The lysates were purified with Ni-NTA super-flow (QIAGEN) followed by glutathione Sepharose 4B (GE Healthcare) according to the manufacturer's instructions.

ATPase Assay

Reaction mixture (25 μl: 1 μg purified recombinant protein, 100 ng RNA, 20 mM Tris–HCl pH 8.0, 1.5 mM $MgCl_2$, 1.5 mM DTT, 20 units Protector RNase Inhibitor (Roche), 1 mM ATP) was incubated at 37°C for 30 min. The product, inorganic phosphate, was quantified with BioMol Green (Enzo).

AFM Observation

AFM imaging of MDA5 was performed utilizing a Nanoscope IIIa/IV with a type E or type J scanner (Digital Instruments) in air with the Tapping Mode at room temperature. The probes used were made of silicon crystal, and the cantilevers were 160 (±20) μm in length with a spring constant of 12–103 Nm $^{-1}$ (OMCL-AC160TS; Olympus). Images were captured with the height mode in a 512 × 512 pixel format at a scanning frequency of 2 Hz. The images obtained were plane-fitted and flattened with the computer program supplied in the imaging module. The three-dimensional surface plots of the pictures were also produced with this program. For observation by AFM, purified WT/mutant MDA5 was diluted in Tris buffer containing 20 mM Tris–Cl (pH 8.0), 1.5 mM $MgCl_2$, and 1.5 mM DTT and was applied to a freshly cleaved mica surface pretreated with 10 mM spermidine. After 10 min, the mica was washed with water and dried with nitrogen gas.

SUPPLEMENTAL INFORMATION

Supplemental Information includes three figures and can be found with this article online at http://dx.doi.org/10.1016/j.immuni.2013.12.014.

ACKNOWLEDGMENTS

This work was supported by independent grants from Japan Science and Technology Agency (PRESTO), from Ministry of Education, Culture, Sports, Science and Technology (MEXT) of Japan (innovative areas, infection competency, no. 24115004 and scientific research A, no. 23249023), from Daiichi Sankyo Foundation of Life Science, and from the Takeda Science Foundation.

Received: July 5, 2013
Accepted: December 16, 2013
Published: February 13, 2014

REFERENCES

Bamming, D., and Horvath, C.M. (2009). Regulation of signal transduction by enzymatically inactive antiviral RNA helicase proteins MDA5, RIG-I, and LGP2. J. Biol. Chem. *284*, 9700–9712.

Banchereau, J., and Pascual, V. (2006). Type I interferon in systemic lupus erythematosus and other autoimmune diseases. Immunity *25*, 383–392.

Beutler, B. (2009). Microbe sensing, positive feedback loops, and the pathogenesis of inflammatory diseases. Immunol. Rev. *227*, 248–263.

Bihl, T., Vassina, E., Boettger, M.K., Goldbach-Mansky, R., Seitz, M., Villiger, P.M., and Simon, H.U. (2005). The T348M mutated form of cryopyrin is associated with defective lipopolysaccharide-induced interleukin 10 production in CINCA syndrome. Ann. Rheum. Dis. *64*, 1380–1381.

Christensen, S.R., Shupe, J., Nickerson, K., Kashgarian, M., Flavell, R.A., and Shlomchik, M.J. (2006). Toll-like receptor 7 and TLR9 dictate autoantibody specificity and have opposing inflammatory and regulatory roles in a murine model of lupus. Immunity *25*, 417–428.

Crampton, S.P., Deane, J.A., Feigenbaum, L., and Bolland, S. (2012). Ifih1 gene dose effect reveals MDA5-mediated chronic type I IFN gene signature, viral resistance, and accelerated autoimmunity. J. Immunol. *188*, 1451–1459.

Dinarello, C.A. (2004). Unraveling the NALP-3/IL-1beta inflammasome: a big lesson from a small mutation. Immunity *20*, 243–244.

Elinav, E., Strowig, T., Henao-Mejia, J., and Flavell, R.A. (2011). Regulation of the antimicrobial response by NLR proteins. Immunity *34*, 665–679.

Gall, A., Treuting, P., Elkon, K.B., Loo, Y.M., Gale, M., Jr., Barber, G.N., and Stetson, D.B. (2012). Autoimmunity initiates in nonhematopoietic cells and progresses via lymphocytes in an interferon-dependent autoimmune disease. Immunity *36*, 120–131.

Gateva, V., Sandling, J.K., Hom, G., Taylor, K.E., Chung, S.A., Sun, X., Ortmann, W., Kosoy, R., Ferreira, R.C., Nordmark, G., et al. (2009). A large-scale replication study identifies TNIP1, PRDM1, JAZF1, UHRF1BP1 and IL10 as risk loci for systemic lupus erythematosus. Nat. Genet. *41*, 1228–1233.

Hoffman, H.M., Mueller, J.L., Broide, D.H., Wanderer, A.A., and Kolodner, R.D. (2001). Mutation of a new gene encoding a putative pyrin-like protein causes familial cold autoinflammatory syndrome and Muckle-Wells syndrome. Nat. Genet. *29*, 301–305.

Hornung, V., Ellegast, J., Kim, S., Brzózka, K., Jung, A., Kato, H., Poeck, H., Akira, S., Conzelmann, K.K., Schlee, M., et al. (2006). 5′-Triphosphate RNA is the ligand for RIG-I. Science *314*, 994–997.

Hugot, J.P., Chamaillard, M., Zouali, H., Lesage, S., Cézard, J.P., Belaiche, J., Almer, S., Tysk, C., O'Morain, C.A., Gassull, M., et al. (2001). Association of NOD2 leucine-rich repeat variants with susceptibility to Crohn's disease. Nature *411*, 599–603.

Imler, J.L., and Hoffmann, J.A. (2001). Toll receptors in innate immunity. Trends Cell Biol. *11*, 304–311.

Kageyama, M., Takahasi, K., Narita, R., Hirai, R., Yoneyama, M., Kato, H., and Fujita, T. (2011). 55 Amino acid linker between helicase and carboxyl terminal domains of RIG-I functions as a critical repression domain and determines inter-domain conformation. Biochem. Biophys. Res. Commun. *415*, 75–81.

Kato, H., Sato, S., Yoneyama, M., Yamamoto, M., Uematsu, S., Matsui, K., Tsujimura, T., Takeda, K., Fujita, T., Takeuchi, O., and Akira, S. (2005). Cell type-specific involvement of RIG-I in antiviral response. Immunity *23*, 19–28.

Kato, H., Takeuchi, O., Sato, S., Yoneyama, M., Yamamoto, M., Matsui, K., Uematsu, S., Jung, A., Kawai, T., Ishii, K.J., et al. (2006). Differential roles of MDA5 and RIG-I helicases in the recognition of RNA viruses. Nature *441*, 101–105.

Kato, H., Takeuchi, O., Mikamo-Satoh, E., Hirai, R., Kawai, T., Matsushita, K., Hiiragi, A., Dermody, T.S., Fujita, T., and Akira, S. (2008). Length-dependent recognition of double-stranded ribonucleic acids by retinoic acid-inducible gene-I and melanoma differentiation-associated gene 5. J. Exp. Med. *205*, 1601–1610.

Kawai, T., and Akira, S. (2011). Toll-like receptors and their crosstalk with other innate receptors in infection and immunity. Immunity *34*, 637–650.

Kawai, T., Takahashi, K., Sato, S., Coban, C., Kumar, H., Kato, H., Ishii, K.J., Takeuchi, O., and Akira, S. (2005). IPS-1, an adaptor triggering RIG-I- and Mda5-mediated type I interferon induction. Nat. Immunol. *6*, 981–988.

Kowalinski, E., Lunardi, T., McCarthy, A.A., Louber, J., Brunel, J., Grigorov, B., Gerlier, D., and Cusack, S. (2011). Structural basis for the activation of innate immune pattern-recognition receptor RIG-I by viral RNA. Cell *147*, 423–435.

Liu, Z., and Davidson, A. (2012). Taming lupus-a new understanding of pathogenesis is leading to clinical advances. Nat. Med. *18*, 871–882.

Meylan, E., Curran, J., Hofmann, K., Moradpour, D., Binder, M., Bartenschlager, R., and Tschopp, J. (2005). Cardif is an adaptor protein in the RIG-I antiviral pathway and is targeted by hepatitis C virus. Nature *437*, 1167–1172.

Nakashima, R., Imura, Y., Kobayashi, S., Yukawa, N., Yoshifuji, H., Nojima, T., Kawabata, D., Ohmura, K., Usui, T., Fujii, T., et al. (2010). The RIG-I-like receptor IFIH1/MDA5 is a dermatomyositis-specific autoantigen identified by the anti-CADM-140 antibody. Rheumatology (Oxford) *49*, 433–440.

Nejentsev, S., Walker, N., Riches, D., Egholm, M., and Todd, J.A. (2009). Rare variants of IFIH1, a gene implicated in antiviral responses, protect against type 1 diabetes. Science *324*, 387–389.

Ogura, Y., Bonen, D.K., Inohara, N., Nicolae, D.L., Chen, F.F., Ramos, R., Britton, H., Moran, T., Karaliuskas, R., Duerr, R.H., et al. (2001). A frameshift mutation in NOD2 associated with susceptibility to Crohn's disease. Nature *411*, 603–606.

Pichlmair, A., Schulz, O., Tan, C.P., Näslund, T.I., Liljeström, P., Weber, F., and Reis e Sousa, C. (2006). RIG-I-mediated antiviral responses to single-stranded RNA bearing 5′-phosphates. Science *314*, 997–1001.

Pisitkun, P., Deane, J.A., Difilippantonio, M.J., Tarasenko, T., Satterthwaite, A.B., and Bolland, S. (2006). Autoreactive B cell responses to RNA-related antigens due to TLR7 gene duplication. Science *312*, 1669–1672.

Robinson, T., Kariuki, S.N., Franek, B.S., Kumabe, M., Kumar, A.A., Badaracco, M., Mikolaitis, R.A., Guerrero, G., Utset, T.O., Drevlow, B.E., et al. (2011). Autoimmune disease risk variant of IFIH1 is associated with increased sensitivity to IFN-α and serologic autoimmunity in lupus patients. J. Immunol. *187*, 1298–1303.

Satoh, T., Kato, H., Kumagai, Y., Yoneyama, M., Sato, S., Matsushita, K., Tsujimura, T., Fujita, T., Akira, S., and Takeuchi, O. (2010). LGP2 is a positive regulator of RIG-I- and MDA5-mediated antiviral responses. Proc. Natl. Acad. Sci. USA *107*, 1512–1517.

Schlee, M., Roth, A., Hornung, V., Hagmann, C.A., Wimmenauer, V., Barchet, W., Coch, C., Janke, M., Mihailovic, A., Wardle, G., et al. (2009). Recognition of 5′ triphosphate by RIG-I helicase requires short blunt double-stranded RNA as contained in panhandle of negative-strand virus. Immunity *31*, 25–34.

Seth, R.B., Sun, L., Ea, C.K., and Chen, Z.J. (2005). Identification and characterization of MAVS, a mitochondrial antiviral signaling protein that activates NF-kappaB and IRF 3. Cell *122*, 669–682.

Shigemoto, T., Kageyama, M., Hirai, R., Zheng, J., Yoneyama, M., and Fujita, T. (2009). Identification of loss of function mutations in human genes encoding RIG-I and MDA5: implications for resistance to type I diabetes. J. Biol. Chem. *284*, 13348–13354.

Stetson, D.B., Ko, J.S., Heidmann, T., and Medzhitov, R. (2008). Trex1 prevents cell-intrinsic initiation of autoimmunity. Cell *134*, 587–598.

Sumpter, R., Jr., Loo, Y.M., Foy, E., Li, K., Yoneyama, M., Fujita, T., Lemon, S.M., and Gale, M., Jr. (2005). Regulating intracellular antiviral defense and permissiveness to hepatitis C virus RNA replication through a cellular RNA helicase, RIG-I. J. Virol. *79*, 2689–2699.

Sun, L., Wu, J., Du, F., Chen, X., and Chen, Z.J. (2013). Cyclic GMP-AMP synthase is a cytosolic DNA sensor that activates the type I interferon pathway. Science *339*, 786–791.

Takahasi, K., Yoneyama, M., Nishihori, T., Hirai, R., Kumeta, H., Narita, R., Gale, M., Jr., Inagaki, F., and Fujita, T. (2008). Nonself RNA-sensing mechanism of RIG-I helicase and activation of antiviral immune responses. Mol. Cell *29*, 428–440.

Toki, H., Inoue, M., Motegi, H., Minowa, O., Kanda, H., Yamamoto, N., Ikeda, A., Karashima, Y., Matsui, J., Kaneda, H., et al. (2013). Novel mouse model for Gardner syndrome generated by a large-scale N-ethyl-N-nitrosourea mutagenesis program. Cancer Sci. *104*, 937–944.

Trinchieri, G. (2010). Type I interferon: friend or foe? J. Exp. Med. *207*, 2053–2063.

Unterholzner, L., Keating, S.E., Baran, M., Horan, K.A., Jensen, S.B., Sharma, S., Sirois, C.M., Jin, T., Latz, E., Xiao, T.S., et al. (2010). IFI16 is an innate immune sensor for intracellular DNA. Nat. Immunol. *11*, 997–1004.

van Heel, D.A., Ghosh, S., Butler, M., Hunt, K.A., Lundberg, A.M., Ahmad, T., McGovern, D.P., Onnie, C., Negoro, K., Goldthorpe, S., et al. (2005). Muramyl dipeptide and toll-like receptor sensitivity in NOD2-associated Crohn's disease. Lancet *365*, 1794–1796.

Wu, B., Peisley, A., Richards, C., Yao, H., Zeng, X., Lin, C., Chu, F., Walz, T., and Hur, S. (2013). Structural basis for dsRNA recognition, filament formation, and antiviral signal activation by MDA5. Cell *152*, 276–289.

Xu, L.G., Wang, Y.Y., Han, K.J., Li, L.Y., Zhai, Z., and Shu, H.B. (2005). VISA is an adapter protein required for virus-triggered IFN-beta signaling. Mol. Cell *19*, 727–740.

Yoneyama, M., and Fujita, T. (2009). RNA recognition and signal transduction by RIG-I-like receptors. Immunol. Rev. *227*, 54–65.

Yoshida, H., Okabe, Y., Kawane, K., Fukuyama, H., and Nagata, S. (2005). Lethal anemia caused by interferon-beta produced in mouse embryos carrying undigested DNA. Nat. Immunol. *6*, 49–56.

Zhang, Z., Yuan, B., Bao, M., Lu, N., Kim, T., and Liu, Y.J. (2011). The helicase DDX41 senses intracellular DNA mediated by the adaptor STING in dendritic cells. Nat. Immunol. *12*, 959–965.

Journal of Virology

Encephalomyocarditis Virus Disrupts Stress Granules, the Critical Platform for Triggering Antiviral Innate Immune Responses

Chen Seng Ng, Michihiko Jogi, Ji-Seung Yoo, Koji Onomoto, Satoshi Koike, Takuya Iwasaki, Mitsutoshi Yoneyama, Hiroki Kato and Takashi Fujita

J. Virol. **2013, 87(17):9511. DOI: 10.1128/JVI.03248-12. Published Ahead of Print 19 June 2013.**

JVI
Journals.ASM.org

Encephalomyocarditis Virus Disrupts Stress Granules, the Critical Platform for Triggering Antiviral Innate Immune Responses

Chen Seng Ng,[a,b] Michihiko Jogi,[a,b,c] Ji-Seung Yoo,[a,b] Koji Onomoto,[a,b,c] Satoshi Koike,[d] Takuya Iwasaki,[d] Mitsutoshi Yoneyama,[a,b,c] Hiroki Kato,[a,b] Takashi Fujita[a,b]

Laboratory of Molecular Genetics, Institute for Virus Research, Kyoto University, Kyoto, Japan[a]; Laboratory of Molecular Cell Biology, Graduate School of Biostudies, Kyoto University, Kyoto, Japan[b]; Division of Molecular Immunology, Medical Mycology Research Center, Chiba University, Chiba, Japan[c]; Neurovirology Project, Tokyo Metropolitan Institute of Medical Science, Tokyo, Japan[d]

In response to stress, cells induce ribonucleoprotein aggregates, termed stress granules (SGs). SGs are transient loci containing translation-stalled mRNA, which is eventually degraded or recycled for translation. Infection of some viruses, including influenza A virus with a deletion of nonstructural protein 1 (IAVΔNS1), induces SG-like protein aggregates. Previously, we showed that IAVΔNS1-induced SGs are required for efficient induction of type I interferon (IFN). Here, we investigated SG formation by different viruses using green fluorescent protein (GFP)-tagged Ras-Gap SH3 domain binding protein 1 (GFP-G3BP1) as an SG probe. HeLa cells stably expressing GFP-G3BP1 were infected with different viruses, and GFP fluorescence was monitored live with time-lapse microscopy. SG formations by different viruses was classified into 4 different patterns: no SG formation, stable SG formation, transient SG formation, and alternate SG formation. We focused on encephalomyocarditis virus (EMCV) infection, which exhibited transient SG formation. We found that EMCV disrupts SGs by cleavage of G3BP1 at late stages of infection (>8 h) through a mechanism similar to that used by poliovirus. Expression of a G3BP1 mutant that is resistant to the cleavage conferred persistent formation of SGs as well as an enhanced induction of IFN and other cytokines at late stages of infection. Additionally, knockdown of endogenous G3BP1 blocked SG formation with an attenuated induction of IFN and potentiated viral replication. Taken together, our findings suggest a critical role of SGs as an antiviral platform and shed light on one of the mechanisms by which a virus interferes with host stress and subsequent antiviral responses.

In eukaryotic cells, viral infections induce several responses. Cellular pathogen recognition receptors such as RIG-I-like receptors (RLRs) and Toll-like receptors recognize specific pathogen-associated molecular patterns and activate the transcription of hundreds of genes, including interferons (IFNs), inflammatory cytokines, and antiviral proteins. Secreted IFNs, in turn, activate a secondary JAK-STAT signaling cascade, which culminates in the activation of various interferon-stimulated genes (ISGs) (1, 2). A representative ISG, protein kinase RNA activated (PKR), acts as an antiviral protein by inducing the blockade of viral translation (3–5). PKR is also known to be associated with the cellular stress responses. Virus infection results in the accumulation of double-stranded RNA (dsRNA), thereby activating PKR and phosphorylation of the α subunit of eukaryotic initiation factor 2 (eIF2α), leading to the formation of stress granules (SGs) (6, 7). Several studies have reported the interaction between viruses and SGs, especially the effects of specific types of viruses on the fate of SG formation and how viruses modulate stress granule assembly (8–11). Recently, we reported that RLR recruitment to SGs during SG formation is critical for RLR-mediated signaling and that nonstructural protein 1 of influenza A virus (IAV) blocks RLR signaling by inhibiting SGs and the antiviral response (12). Accumulating evidence suggests that viruses have evolved strategies to prevent SG formation. These results suggest that virus-induced SGs potentially serve as platforms for antiviral activity; however, the underlying molecular mechanism still remains to be elucidated.

In the present study, we aim to delineate the physiological impact of stress granule formation and its viral modulation. We employed an enhanced green fluorescent protein (EGFP)-tagged stress granule marker, Ras-Gap SH3 domain binding protein 1 (G3BP1), to probe the subcellular distribution of virus-induced SGs (13, 14). This system allows us to monitor SGs in an individual virus-infected cell. Infection with RNA and DNA viruses displayed three distinct patterns: stable, transient, and alternate formation of SGs. We focused on encephalomyocarditis virus (EMCV), which exhibited transient formation of SGs. We show that EMCV disrupts SGs through G3BP1 cleavage. Furthermore, we found that EMCV-induced SGs are required for efficient activation of IFN and cytokine genes. We propose a new antiviral concept highlighting the potential cross talk of virus-induced stress responses and activation of the IFN signaling cascade. This may provide new insight into understanding the mechanism by which antiviral genes are regulated.

MATERIALS AND METHODS

Plasmid constructs. The stress granule marker constructs pEGFP-C1-G3BP1 (NCBI RefSeq accession no. NM_005754) was a kind gift from Jamal Tazi (Institute de Génétique Moléculaire de Montpellier, France). The pEGFP-C1-G3BP1 Q325E mutant construct was generated by site-directed mutagenesis with a KOD-Plus mutagenesis kit (Toyobo, Japan) using primers containing the desired mutation according to manufacturer's instructions and were completely sequenced by using an ABI Prism

Received 22 November 2012 Accepted 6 June 2013
Published ahead of print 19 June 2013
Address correspondence to Takashi Fujita, tfujita@virus.kyoto-u.ac.jp.
Supplemental material for this article may be found at http://dx.doi.org/10.1128/JVI.03248-12.

doi:10.1128/JVI.03248-12

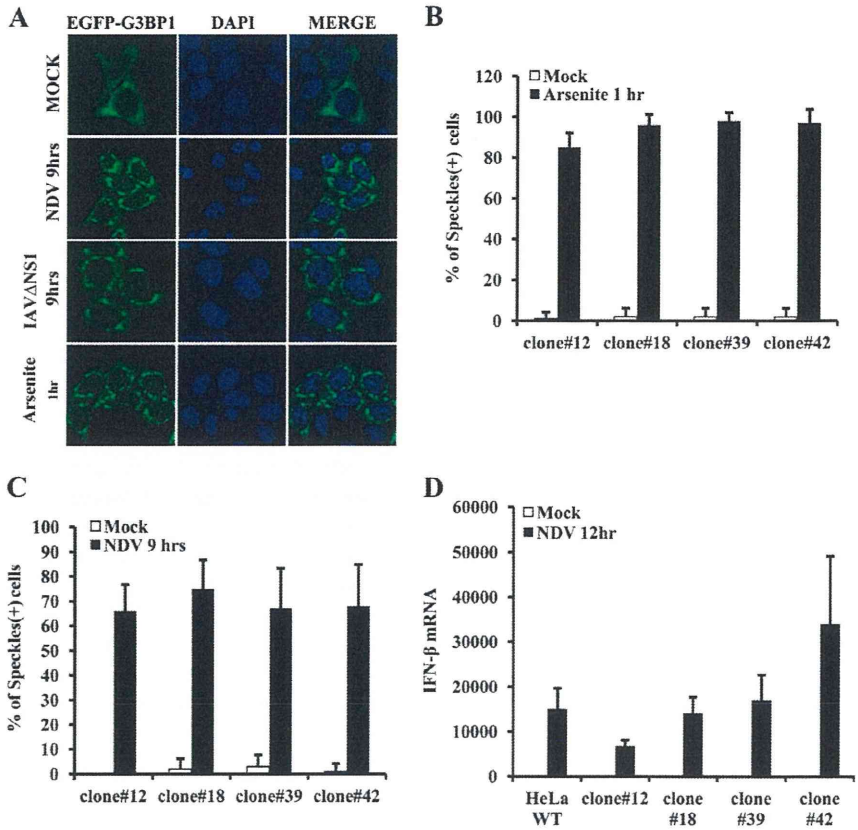

FIG 1 Characterization of HeLa/G-G3BP cells. (A) HeLa/G-G3BP1 clone 12 was mock treated or stimulated, as indicated. DAPI, 4′,6-diamidino-2-phenylindole. (B and C) Cells were fixed and examined for GFP fluorescence. Four independent HeLa/G-G3BP cell clones were stimulated by arsenite (B) or by infection with NDV (C), and the percentage of GFP speckle-positive cells was determined. (D) Parental HeLa cells and HeLa/G-G3BP1 clones were infected with NDV for 12 h, and the IFN-β gene expression level was determined by RT-qPCR. (Error bars indicate standard deviations of duplicates [$n = 2$].)

DNA sequencer to verify the presence of the mutation. This plasmid contained a single-point amino acid substitution at position 325 (from glutamine to glutamate), which is resistant to cleavage by $3C^{PRO}$ of poliovirus (PolioV) (15). Expression vectors for EMCV pFirefly-leader and pFirefly-3C proteases were described previously (16).

Viruses. PolioV (Mahoney strain), vesicular stomatitis virus (VSV) (Indiana strain), EMCV, adenoviruses (type 5), Sindbis virus (SINV), and Theiler's murine encephalomyelitis virus (TMEV) (GDVII strain) were prepared by infecting BHK cells at a multiplicity of infection (MOI) of 1. Cell culture medium was collected after confirming cytopathic effects following infection. Medium containing newly produced viruses was centrifuged at 1,500 rpm for 5 min to pellet the cell debris, and supernatants containing viruses were collected and stored at −80°C. The viral titer was assessed by a plaque assay on L929 cells, as previously described (17). Newcastle disease virus (NDV) (Miyadera strain), Sendai virus (SeV) (Cantell), and influenza A virus with a deletion of the NS1 gene (IAVΔNS1) (strain A/Puerto Rico 8/34) (18, 19) were propagated in the allantoic cavities of embryonated chicken eggs, and stocks were then stored at −80°C.

Generation of stable HeLa cells and general cell culture conditions. Cell lines were maintained in Dulbecco's modified Eagle's medium (DMEM) supplemented with 10% heat-inactivated fetal bovine serum (Nacalai Tesque, Japan) and penicillin-streptomycin (100 U/ml and 100 μg/ml, respectively; Nacalai Tesque, Japan). To generate HeLa cells stably expressing the EGFP-G3BP1 wild type (wt) and the EGFP-G3BP1 Q325E mutant, pEGFP-C1-G3BP1 and pEGFP-C1-G3BP1 Q325E mutant expression constructs were linearized by using the restriction enzyme ApaLI (TaKaRa, Japan). The linearized plasmids were then transfected into HeLa cells by using FuGENE6 (Promega, USA) according to manufacturer's recommendations. Transformants were selected by including 1 mg/ml of G418 in the culture medium. Individual colonies were isolated and characterized.

Live-cell imaging and immunofluorescence microscopy. For the live-cell imaging analysis, HeLa cells stably expressing EGFP-G3BP1 (HeLa/G-G3BP cells) were seeded into a 12-well plate and incubated at 37°C. After 24 h, cells were washed with DMEM (10% fetal bovine serum and 1% penicillin-streptomycin) for several rounds. Cells were then infected with various types of RNA and DNA viruses. After 1 h of infection, virus was removed and replaced with 1.0 ml of DMEM imaging medium (4,500 mg/liter D-glucose and L-glutamine, 25 mM HEPES buffer, no sodium pyruvate, and phenol red; Invitrogen). Imaging was immediately initiated every 10 min. Live cells were maintained on the microscope stage at 37°C with 5% carbon dioxide in a humidity-controlled chamber. Images were taken by using Biophotonics-ImageJ software. All imaging was performed by using a Leica CTR 6500 instrument.

For the immunofluorescence analysis, cells were seeded into either a 12-well plate or an 8-well chamber slide and incubated at 37°C. After 24 h, cells were subjected to various treatments, such as plasmid transfection or virus infection. Cells were then rinsed in phosphate-buffered saline (PBS) several times, fixed with 4% paraformaldehyde solution for 10 min at room temperature, washed with PBS for two additional rounds, permeabilized with acetone-methanol (1:1) for 1 min, and blocked with phosphate-buffered saline containing 0.1% Tween 20 (PBST) and containing bovine serum albumin (BSA) (5.0 mg/ml) for 1 h at 4°C. Cells were then

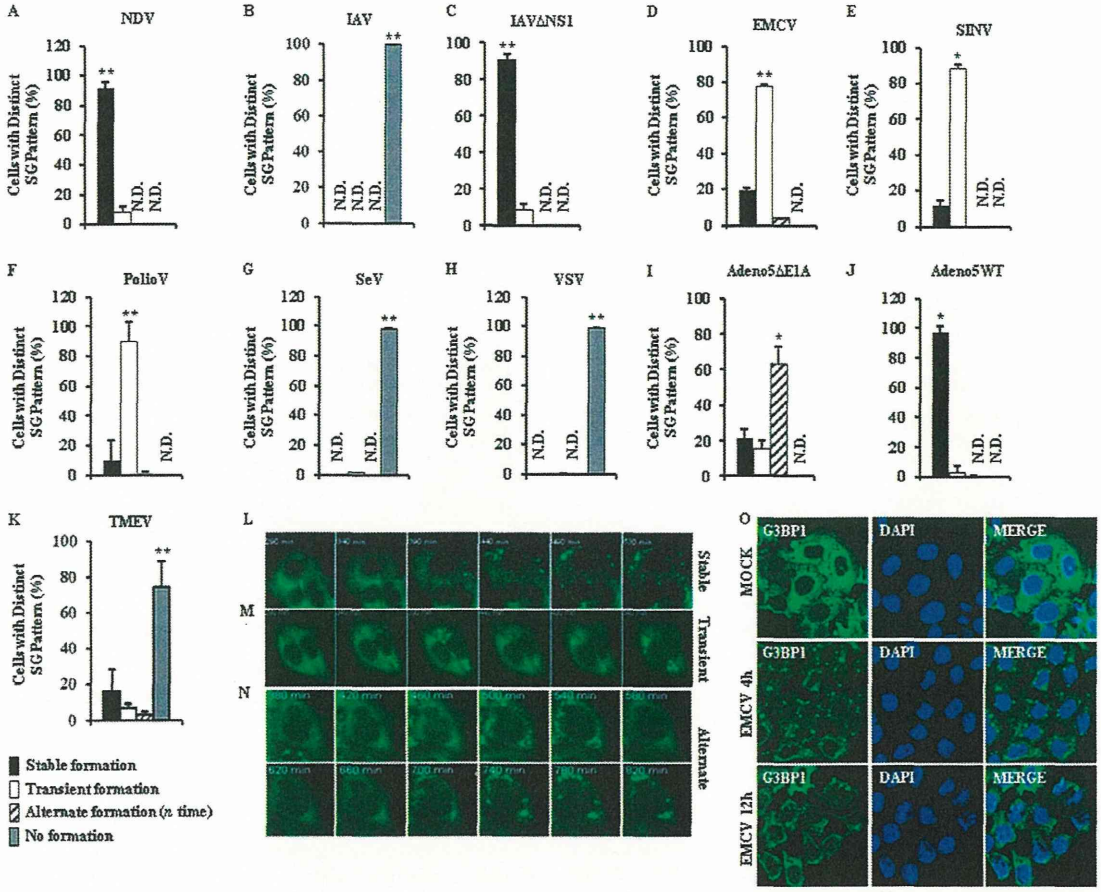

FIG 2 Three major forms of virus-induced stress granule distribution patterns in HeLa/G-G3BP cells infected with different viruses. (A to K) HeLa/G-G3BP cells were infected with NDV (A), IAV (B), IAVΔNS1 (C), EMCV (D), SINV (E), PolioV (F), SeV (G), VSV (H), adenovirus type 5 with an E1A deletion (Adeno5ΔE1A) (I), wild-type adenovirus type 5 (Adeno5WT) (J), and TMEV (K) for approximately 9 to 12 h, and SG formation was monitored and quantified as described in Materials and Methods. (Error bars indicate standard deviations of triplicates [$n = 3$].) N.D., not detectable; **, $P < 0.005$; *, $P < 0.05$. (L to N) Representative cell images taken at the indicated times after infection for stable (NDV) (L), transient (SINV) (M), and alternating (Adeno5ΔE1A) (N) SG formation. (O) Wild-type HeLa cells were mock infected or infected for 4 or 12 h and fixed to examine the localization of endogenous G3BP1 by immunostaining.

incubated with primary antibody followed by fluorophore-conjugated secondary antibodies (Invitrogen) for 1 h at 4°C. Cells were washed with PBST extensively and mounted. All images were obtained by using a Leica CTR 6500 instrument.

siRNA-directed gene silencing. The small interfering RNA (siRNA) universal negative control and siRNAs targeting the stress granule marker G3BP1 (50 nM) and the dsRNA protein kinase PKR were purchased from Invitrogen and transfected by using either Lipofectamine 2000 (Invitrogen) or RNAiMax (Invitrogen) according to the manufacturer's recommendations. The sequences of siRNAs are as follows: sense sequence 5′-CGG AUU AGC GAC AAA UUU AUU-3′ and antisense sequence 5′-UAA AUU UGU CGC UAA UCC GUU-3′ for RIG-I, sense sequence 5′-UUU ACU UCA CGC UCC GCC UUC UCG U-3′ and antisense sequence 5′-ACG AGA AGG CGG AGCGUGAAGUAA A-3′ for PKR#1, sense sequence 5′-AUG UCA GGA AGG UCA AAU CUG GGU G-3′ and antisense sequence 5′-CAC CCA GAU UUG ACC UUC CUG ACA U-3′ for PKR#2 (#*n*, designated siRNA number), and sense sequence 5′-UAA UUU CCC ACC ACU GUU AAU GCG C-3′ and antisense sequence 5′-GCGCAUUAACAGUGGUGGGAAAUUA-3′ for G3BP1. At 48 h post-transfection, cells were subjected to viral infection or other treatments. A specific antibody for G3BP1 (Santa Cruz) was used to monitor the knockdown efficiency.

RNA analysis. RNA was harvested from cells by using TRIzol (Invitrogen) according to the manufacturer's instructions. Contaminating DNA was then eliminated by using recombinant DNase I (10 units/μl; Roche) according to the manufacturer's protocol. Treated samples were purified by phenol-chloroform extraction. Five hundred nanograms of purified RNA was used as a template to synthesize cDNA by using a High Capacity cDNA reverse transcription kit (Applied Biosystems), as specified by the manufacturer, with the following cycles: 25°C for 10 s, 37°C for 2 h, and 85°C for 10 s. The concentration of cDNA was quantified by the use of a spectrophotometer, and the final concentration was adjusted to 1 μg/μl. cDNA samples were then subjected to either standard PCR or real-time quantitative PCR (RT-qPCR) analysis with specific probes from the TaqMan gene expression assay (Applied Biosystems). Quantification of EMCV RNA was performed by using SYBR master mix (Applied Biosystems) with specific primers targeting the EMCV capsid coding region. Standard PCR was performed with cDNA samples together with a master mix containing 1× PCR buffer, 2.5 mM each deoxynucleoside triphosphates (dNTPs), 0.2 units of Ex *Taq* polymerase, and 1.0 μM both forward and reverse primers. PCR buffer, dNTPs, and Ex *Taq* polymerase were purchased from TaKaRa, Japan. Primers were all customized and purchased from Invitrogen. PCR was performed with a 50-μl reaction mix-

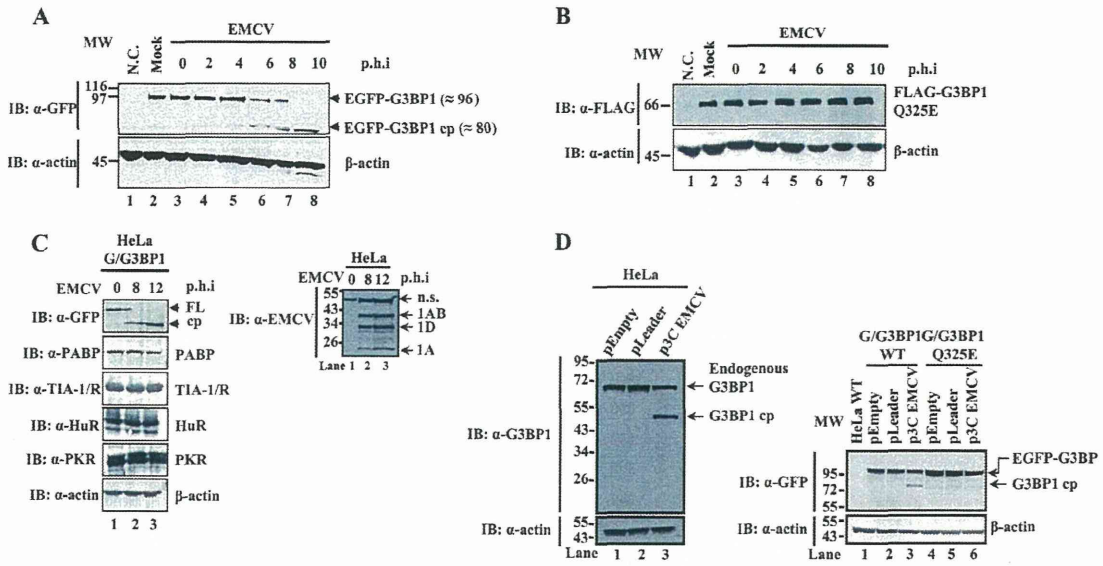

FIG 3 EMCV infection results in the cleavage of G3BP1. (A) Immunoblotting (IB) showing the kinetics of G3BP1 cleavage in EMCV-infected HeLa/G-G3BP1 cells. N.C., negative control. (B) HeLa cells stably expressing FLAG-G3BP1 Q325E protein were infected with EMCV, and the G3BP1 Q325E protein level was monitored by immunoblotting. (C) Western blot analysis of HeLa/G-G3BP1 cells infected with EMCV. Lysates were prepared at the indicated time points after infection and subjected to immunoblotting with the indicated antibodies. FL, full-length; n.s., not significant. (D, left) HeLa cells were transiently transfected with an empty vector or the expression vector for leader or 3C and analyzed for endogenous G3BP1 by Western blotting. (Right) HeLa/G-G3BP1 and HeLa/G-G3BP1Q325E cells were transiently transfected with an empty vector or the expression vector for leader or 3C and analyzed by Western blotting using anti-GFP. MW, molecular weight (in thousands); p.h.i., hour postinfection; cp, cleavage fragment.

ture with an initial annealing temperature of 56°C to 60°C. PCR products were analyzed by agarose gel electrophoresis.

Western blotting. Cells were collected in ice-cold PBS by using a scraper. Cells were collected by centrifugation and lysed by NP-40 buffer (50 mM Tris [pH 8.0], 150 mM NaCl, 1% [vol/vol] NP-40, 1 nM vanadate, 1 mM leupeptin, and phenylmethanesulfonyl fluoride), followed by centrifugation at 15,000 rpm for 10 min and ultracentrifugation at 100,000 rpm for 5 min. The supernatant was mixed with an equal volume of 2× SDS buffer, boiled for 5 min, separated by SDS-PAGE (30 μg/lane), and transferred onto a nitrocellulose membrane. The membranes were incubated in blocking buffer (PBS, 5% [wt/vol] dry milk powder) for 30 min at room temperature, followed by incubation with primary antibody diluted in blocking buffer at 4°C overnight. Membranes were washed extensively with TBST (Tris-buffered saline, 0.1% Tween 20), followed by incubation with a conjugated secondary antibody for 1 h at room temperature. The proteins were visualized by using alkaline phosphatase buffer containing 5'-bromo-4-chloro-3'-indolylphosphate (BCIP)-Nitro Blue Tetrazolium (NBT) (Promega) color development substrate (100 mM

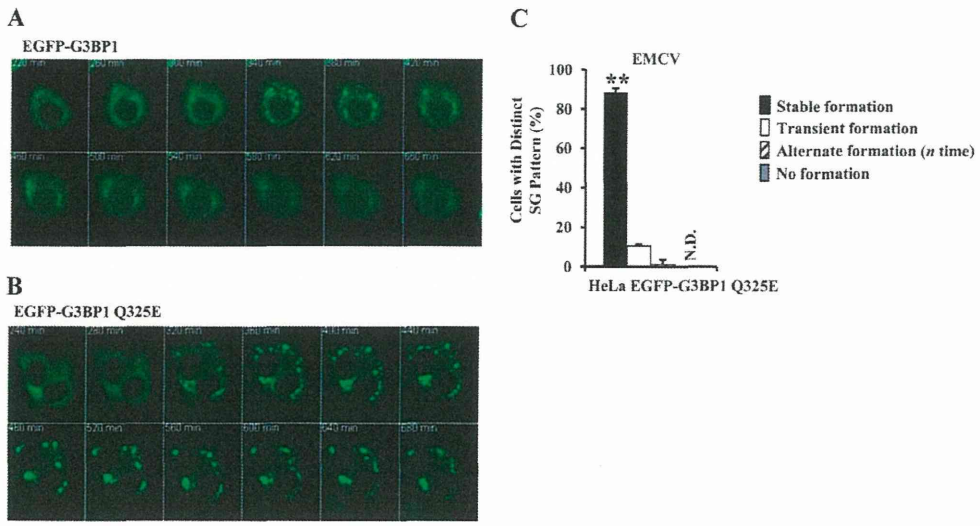

FIG 4 HeLa/G-G3BPQ325E cells display stable formation of SGs induced by EMCV infection. (A and B) Both HeLa/G-G3BP1 (A) and HeLa/G-G3BP1Q325E (B) cells were infected with EMCV. GFP fluorescence images of these cells taken every 40 min are shown. (C) Quantitative analysis of SG formation pattern of HeLa/G-G3BP1Q325E cells infected with EMCV. (Error bars indicate standard deviations of triplicates [$n = 3$].) N.D., not detectable; **, $P < 0.005$.